J Mol Model (2008) 14:451–464
DOI 10.1007/s00894-008-0296-x

ORIGINAL PAPER

# Probing the interactions of the solvated electron with DNA by molecular dynamics simulations: bromodeoxyuridine substituted DNA

**Tsvetan G. Gantchev · Darel J. Hunting**

Received: 13 November 2007 / Accepted: 28 February 2008 / Published online: 15 April 2008


**Abstract** Solvated electrons ($e^-_{aq}$) are produced during water radiolysis and can interact with biological substrates, including DNA. To augment DNA damage, radiosensitizers such as bromo-deoxyuridine (BUdR), often referred to as an "electron affinic radiosensitizer", are incorporated in place of isosteric thymidine. However, little is known about the primary interactions of $e^-_{aq}$ with DNA. In the present study we addressed this problem by applying molecular modeling and molecular dynamics (MD) simulations to a system of normal (BUdR·A)-DNA and a hydrated electron, where the excess electron was modeled as a localized $e^-(H_2O)_6$ anionic cluster. Our goals were to evaluate the suitability of the MD simulations for this application; to characterize the motion of $e^-_{aq}$ around DNA (e.g., diffusion coefficients); to identify and describe configurational states of close $e^-_{aq}$ localization to DNA; and to evaluate the structural dynamics of DNA in the presence of $e^-_{aq}$. The results indicate that $e^-_{aq}$ has distinct space-preferences for forming close contacts with DNA and is more likely to interact directly with nucleotides other than BUdR. Several classes of DNA - $e^-_{aq}$ contact sites, all within the major groove, were distinguished depending on the structure of the intermediate water layer H-bonding pattern (or its absence, i.e., a direct H-bonding of $e^-_{aq}$ with DNA bases). Large-scale structural perturbations were identified during and after the $e^-_{aq}$ approached the DNA from the major groove side, coupled with deeper penetration of sodium counterions in the minor groove.

T. G. Gantchev (✉) · D. J. Hunting
Department of Nuclear Medicine & Radiobiology,
Faculty of Medicine, Université de Sherbrooke,
Sherbrooke, QC J1H 5N4, Canada
e-mail: tsvetan.gantchev@usherbrooke.ca

**Keywords** Bromodeoxyuridine (BUdR) · DNA conformation · Electron attachment · Hydrated electron · Molecular dynamics · Molecular modeling · Radiosensitization

## Introduction

Hydrated electrons, $e^-_{aq}$ are a major species produced during water radiolysis with a radiation yield as high as that of ·OH radicals ($G=2.8\times10^{-7}$ mol $J^{-1}$) [1]. During the last decade, the intriguing structural and optical properties of $e^-_{aq}$ [2], and more generally the solution chemistry of excess electrons in molecular liquids have received growing attention by theoreticians [3–8] and spectroscopists [9–12]. Studies of anionic water clusters presuppose solvated electron structural models of various hierarchy, $e^-(H_2O)_n$, n=6–50 and many have been tested to different extents experimentally. Regardless of the alternative $e^-_{aq}$ models, e.g., $(OH^-\ldots H_3O)_{aq}$ type complexes [13], the $e^-$ + $6H_2O$ (Kevan's, one shell [14, 15]), and the $e^-$ + $(6+12)H_2O$ (two shells), the concept of localized or cavity anions has been well supported by spectroscopic and theoretical calculations and remains the most popular.

Hydrated electrons can efficiently interact with nucleobases and isolated nucleotides, with bimolecular rate constants in the range of $(0.9–1.7)\times10^{10}$ $M^{-1}s^{-1}$ [1]. In purified DNA, the decrease of reaction efficiency is about two orders of magnitude compared with isolated nucleotides [1]. The exact reasons behind this decline are not known, but it is safe to assume that the macromolecular structure at all levels (primary, secondary and tertiary) together with the DNA and Debay-Hückel layer dynamics play a role in the modulation of reactivity. During the last several years, studies on excess electron transfer in DNA

have provided significant insights into the molecular mechanisms of DNA damage induced in model systems [16–19]. However, no mechanistic details concerning the primary interaction of $e^-_{aq}$ with nucleobases and DNA are available.

Replacement of thymidine by isosteric 5-bromodeoxyuridine (BUdR) sensitizes DNA to damage by γ-radiolysis ($e^-_{aq}$) and UV photolysis [1]. It has long been known that this process involves one-electron reduction of BUdR followed by dissociative cleavage of the C(5)—Br bond and release of $Br^-$ (or $Br^{\cdot}$ in UV photolysis). The ensuing vinyl-type $U^{\cdot}$ radical is highly reactive, and eventually abstracts a hydrogen atom from deoxyribose on the same (brominated) strand, e.g., from the C2′ position of the 5′-adjacent nucleotide [20], ultimately resulting in a DNA strand break. However, BUdR radiosensitization is likely more complicated because of the concomitant process of charge transfer (CT) in DNA [21]. The intervention of CT may occur in two instances. In DNA, it is unknown whether the production of the $BU^-$ anion is a result of a preferential and directed capture of $e^-_{aq}$ by BUdR, or whether the electron initially reduces other nucleobases (e.g., T, C or A), followed by an excess electron transfer to BUdR [22, 23]. In the latter case, the role of BUdR is that of an electron trap for the already DNA-localized electron, but it is not the "antenna" which initially interacts with the $e^-_{aq}$. Secondly, the resulting uracil-5-yl radical, $U^{\cdot}$ may act as an electron acceptor, thus initiating a hole transfer along the DNA. Therefore, a migration of the DNA lesion from the primary BUdR site may take place. Indeed, in our recent DNA radiosensitization studies with selected oligonucleotides which hybridize to normal, or wobble (mismatched) BUdR-containing DNA duplexes, we have found that strand breaks are preferentially formed at several sites on the brominated or non-brominated strand (but never on both) [24, 25]. In addition, in wobble DNA, high efficiency, $e^-_{aq}$ - mediated formation of interstrand crosslinks takes place, involving nucleotides that can be proximal or distant to BUdR [25, 26]. This implies a contribution of specific CT or HT processes, initiated by the primary $e^-_{aq}$ attachment to DNA (not necessarily to BUdR only), and followed by an array of CT steps which are likely controlled by local DNA structure and dynamics. Using molecular dynamics (MD) simulations, we have further shown that, in contrast to normal DNA, the dynamic structure of mismatched DNA is prone to frequent cross-strand inter-base atom encounters [27].

In a continuation of our previous molecular dynamics study we present here results from 2 ns MD simulations of fully hydrated normal DNA duplex with incorporated BUdR, and in the presence of $e^-_{aq}$, modeled as an $e^-(H_2O)_6$ cluster. We have undertaken this *in silico* approach with the following goals: i) to set up a DNA-$e^-_{aq}$ model system suitable for analysis of the thermalized $e^-_{aq}$ motion around DNA; ii) to characterize $e^-(H_2O)_6$ hydrodynamic parameters in a micro-heterogeneous environment; iii) to evaluate system configuration states when $e^-_{aq}$ is in close contact with DNA; iv) to identify any preferences for the interaction of $e^-_{aq}$ with BUdR; and v) to investigate the extent to which the canonical DNA structure is perturbed by $e^-_{aq}$.

## Computational methods

All molecular modeling tasks and computations were carried out using Tripos Inc. Expert Molecular Modeling Environment package, Sybyl 7.2–8.0 running on MIPS10000 IP30 SGI Octane (IRIX 6.5.26) or IBM Pentium 4 RedHat Enterprise (LINUX 4.0) platforms. During this work we used Sybyl quantum (MOPAC) and molecular mechanics (MAXIMIN2) modules; Silverware solvation program with Amber7 Force Field engine, Biopolymer and Molecular Dynamics modules. Electronic surfaces were calculated using MOLCAD. The molecular structures were built and prepared for the Newtonian molecular dynamics simulations as follows:

1. *Solvated electron*: The hydrated electron is presented as an $e^-(H_2O)_6$ cluster, i.e., Kevan's structural (single water shell) model. In the initial geometry the cavity was left unmodified and fixed to the original parameters as defined by Kevan and co-workers: a regular octahedral arrangement of six water molecules with an O—H pointing toward the center of the cavity with the distance of the cavity center to the first hydrogen= 2.1 Å [14]. This structure was subjected to UHF and HF-C.I. MO computations using AM1 *semi*-empirical Hamiltonian (MOPAC6.0, QCPE # 455) applying full or restricted ($C_i$) geometry optimization and Mulliken partial charge analysis. Successful convergence (BGFS gradients and SCF) was achieved with several slightly different $e^-(H_2O)_6$ geometries (e.g., smaller cavity dimensions) with ΔH falling in the range from −304 to −345 kcal $mol^{-1}$. From these computations and the HOMO/SOMO/LUMO energies (1s-ground state and three nearly degenerated p-states) we estimated the ionization potential, IP ~ 2.3 eV and first excited state, $E_{(0\rightarrow1)}$ ~ 1.7 eV. These values correspond well to the known experimental data and those computed by ab initio methods [6]. In the MD simulations we have chosen to use the most symmetric original structure with Mulliken charges (assigned as formal charges) and have imposed 12 distance constraints, so that each inner hydrogen atom is bound to its four nearest neighbors with harmonic oscillator force constants of 10 kcal

$mol^{-1}$ $Å^{-2}$ (in the preparative MD stages) further relaxed to 1 kcal $mol^{-1}$ $Å^{-2}$ in the course of MD production runs. Before and after solute hydration the $e^{-}(H_2O)_6$ geometry was again optimized using MM (Amber7_FF99 force field).

2. *DNA structure, hydration and counter ions*: The starting 11-mer duplex DNA contained a central 5′d (TTT)·d(AAA) triplet and GC clamps close to its ends. The complete sequence was 5′d(ACGATTTACGA)·d (TCGTAAATCGT). The T-base in the central pair, T (6)·A(17) was mutated to incorporate bromo-deoxyuridine, T(6) → BU(6) (brominated strand). The resulting sequence was part of the truncated 25-mer oligonucleotide used in our radiosensitization experiments to study DNA breaks and inter-strand crosslinks [24, 25]. The DNA molecular simulation data presented in this work refer to the DNA molecule of the sequence 5′d (ACGATBUTACGA)·d(TCGTAAATCGT) with a central base pair, BU(6)·A(17) presenting a canonical Watson-Crick H-bonding. The initial canonical B-type structures were built and minimized essentially following the procedures described in our previous work with distance-dependent dielectric constant (D=4) [27], but using updated AMBER7_FF99 Force Field. The AMBER7_FF99 parameterized BUdR structure was added previously to the custom-built Sybyl biopolymer monomer dictionary [27]. In the following step, DNA charges were neutralized by 20 sodium counterions positioned 6 Å from the P atoms along the bisector of the backbone OPO [28], initially constrained applying a harmonic constant of 100 kcal $mol^{-1}$ $Å^{-2}$ and briefly minimized (Steepest Descent Algorithm). To maintain an ionic strength of ~ 0.1 M after hydration, three additional $Na^+/Cl^-$ ion pairs, plus a $Na^+$ ion to compensate the electron charge were added near the DNA ends. Hydration was performed using the Sybyl Silverware module in a rectangular box with dimensions of approx. 38×38×49 Å (set as minimal periodic boundary conditions, PBC). During different trials, hydration iterations accomplished at a density of ~1.37 g/$cm^3$, after adding ~2800–2900 water molecules. Following the hydration procedure, geometry was extensively optimized using the unconstrained conjugated gradient algorithm. Typically, minimizations completed at a system potential energy of about $-2.5\times10^4$ kcal $mol^{-1}$, to which the contribution of DNA was about - 400 kcal $mol^{-1}$. Next, the hydrated electron, represented by the $^{-}(H_2O)_6$ water cluster and built as explained above, was added to the system. This was performed by selecting and removing six water molecules located in a sphere of a radius ~3 Å and a center at a distance of 22 Å from the lower PBC corner facing the 5d′(C13G14) backbone edge of the non-brominated DNA strand, at ~7 Å from the nearest P-atom (Fig. 1). Following new energy minimizations, with $e^{-}(H_2O)_6$ and $Na^+$ ions around the DNA minor groove again heavily constrained, the completed hydrated DNA - $e^{-}_{aq}$ systems were submitted to MD simulations as described below.
3. *Molecular dynamics protocol*: MD simulations encompass two stages: preparative and production runs. We employed the preparation protocol recommended by Westhof et al. [29] with some modifications. To relax possible strains between hydration water molecules in all investigated DNA systems (with or without embedded $e^{-}_{aq}$) a brief 1 ps MD was run at 10 K and constant volume (canonical N, T, V ensemble) with DNA, $e^{-}_{aq}$ and counterions fixed to their initial positions (i.e., aggregates), followed by new unconstrained conjugated gradient geometry optimization. Then the water bath was again gradually thermalized to 250 K in steps of 50 K (solute atoms fixed) and rapidly cooled down to 0 K. Before the subsequent constant pressure (isobaric N, T, P ensemble) heating phase set to 250 K, the $Na^+$ - P atom distance constraints were re-invoked (k=10 kcal $mol^{-1}$ $Å^{-2}$) and range constraints (1.8 – 2.5 Å) on each Watson-Crick H-bond (k=4 kcal $mol^{-1}$ $Å^{-2}$) were defined. Additionally, to reinforce the B-type DNA conformation during heating, Δ-torsional angles were weakly constrained to 140 deg (k=5 kcal $mol^{-1}$ $rad^{-2}$). To avoid "frying" DNA ends, the edge base-pairs were maintained as standstill aggregates. The $e^{-}(H_2O)_6$ inward H-atoms were bound by harmonic constants of

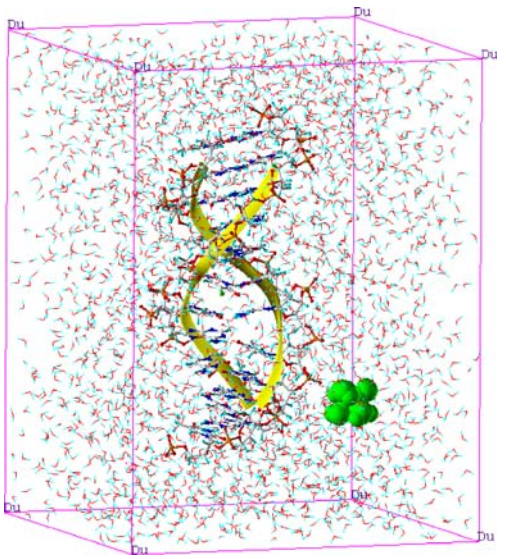


**Fig. 1** Starting configuration of a complete system prior to the 2 ns MD run: PBC box (magenta); hydration water and DNA color-coded by atom types; sodium atoms (magenta); chlorine atoms (blue-green); BU(6)·A(17) is at the middle of the duplex; Br-atom (green). Hydrated electron as an $e^{-}(H_2O)_6$ cluster (green; space fill presentation); DNA backbone (yellow ribbon)

10 kcal mol$^{-1}$ Å$^{-2}$. Heating was performed again in steps of 50 K, 2 ps each, except the end step at 250 K which was 6 ps long. The simulation temperature was set to 250 K to keep a glassy-matrix environment at 1 atm external pressure and compressibility of 45.84×10$^{-6}$ atm$^{-1}$ [30]. This temperature was selected also to correspond to the experimental conditions typically used to study $e^-_{aq}$ interactions with DNA. The MD simulation was stopped at 2 ns for several reasons, including: i) analyses showed that during this interval, $e^-(H_2O)_6$ visited the free space around DNA in all directions; ii) longer MD times would be unrealistic, since $e^-_{aq}$ reacts with DNA in a time-course of 2–3 ns, while every few nanoseconds, a new $e^-_{aq}$ could be generated in this volume under irradiation. Other typical MM parameters used were: standard Amber7 VdW atomic radii and atom charges; constant dielectric function with D=1; NB-cutoff=9 Å; NB-update = 10 fs; integration step = 2 fs; system snap-shots every 500 fs; coupling factors during the heating stage of 100 fs (T), 300 fs (P) and2` 500 fs (P) (during the production runs). Particle-Mesh-Ewald (PME) [31] is not accessible in Sybyl Amber7 version and was not used. Therefore, long-range Coulombic interactions were trimmed by applying 1–4 scaling of the E(tot) electrostatic term by a factor of 0.6, while the H-bond radius was not scaled. These settings, together with the relatively frequent update of the non-bonded pair list (10 fs), were assumed to comply sufficiently with the dimensions of the studied system [32, 33]. The SHAKE algorithm was applied during entire MD runs to enforce harmonic constraints on H-covalent bonds (tolerance of 0.0005 Å). The heating stage was followed by a relaxation stage during which all imposed distance and dihedral constraints were gradually reduced to zero (in steps of 2 ps), except for the 12 distance constraints between inner H-atoms of the $e^-(H_2O)_6$ which remained distance-constrained with a harmonic constant of 1 kcal mol$^{-1}$ Å$^{-2}$. It is noteworthy that during the heating/relaxation stages there were no major DNA and $e^-(H_2O)_6$ constraint violations (except for the counter-ions, which were quite mobile), indicating that the studied systems were well equilibrated. Finally, before the production MD run, the system was checked again during an equilibrium stage of ~30 ps. Total prolongation of the preparative phase was ~50 ps, thereafter the following 2000 ps were part of the production MD and the output subjected to various analyses.

4. *Analysis of the MD results*: The analyses of the configurational/conformational states of the different studied systems (MD time-frames of 0.5 ps), including DNA conformations, $e^-_{aq}$ mobility and residence sites, thermodynamic parameters, etc. were performed using the dynamics table (spreadsheet) and Sybyl graphics tools [27]. The most often used options were: i) filling the dynamics table with custom columns: in addition to the standard thermodynamic output in the dynamics table, we calculated new columns (>250) with canonical DNA angles, torsions and interatomic distances, distances between DNA (NB and PO atoms) and $e^-_{aq}$ outward H-atoms, absolute displacement of the center of mass (XYZ_Abs) of $e^-_{aq}$ and counter-ions, etc. XYZ_Abs represents the motion of an individual atom, or a group of atoms from a chosen initial position; ii) plotting and interactively analyzing the corresponding trajectories in 2D and 3D co-ordinate systems, etc; iii) the analyses were further facilitated by the Tripos-spreadsheet selection tools, which allow one to extract from between the 4000 table rows (MD frames) those complying with a given rule, e.g., minimum numerical value range, coupled by interactive 3D-structure visualization, creating molecular databases of selected system configurations, further subjected to detailed analyses, etc. Electron hydrodynamics was characterized by calculating mean values of the radius of gyration ($RAD_{GYR}$), structure deformability (mass weighted RMS-deviation, $DEF_{ABS}$) and diffusion coefficient, $D(e^-_{aq})$. The later was calculated from the Einstein's formula: $<[X_i(t+\Delta t) - X_i(t)]^2>=6D.\Delta t$. Data were extracted from linear trajectory segments of the XYZ_Abs plot avoiding sites of transient immobilization near DNA. Throughout this study the molecular energy values are given in kcal mol$^{-1}$ (Sybyl default; 1 J=1.4×10$^{20}$ kcal mol$^{-1}$ and 1 kcal mol$^{-1}$=0.0435 eV).
5. *System dynamics (an overview)*: A general analysis of the 2 ns MD runs was performed by plotting trajectories of thermodynamic parameters (V, T, P), water density, potential (PE), kinetic (KE), total (TE) energies, etc. and computing their mean values and statistical variations (Fig. 2 and Table 1). Over the time course of all simulations, trajectories were smooth and fluctuations were within acceptable ranges, indicating the absence of severe abnormalities, such as translational/rotational motion of any system component that would lead to artificial interactions with periodic images. Similarly, thermodynamic and hydrodynamic parameters of the $e^-_{aq}$ were analyzed (alone and in the presence of DNA) (Fig. 2 and Table 1). In the absence of $e^-_{aq}$, the MD outputs with DNA did not indicate any deformability and the DNA structure and counter-ion mobility were consistent with the reported results [34–37]; however, in the presence of $e^-_{aq}$ deformations of DNA were obvious and involved severe distortion of the canonical Watson-Crick (WC) H-bonding pattern, unusual base pair propeller twist, high stagger, opening, etc, as is described in the Results section.

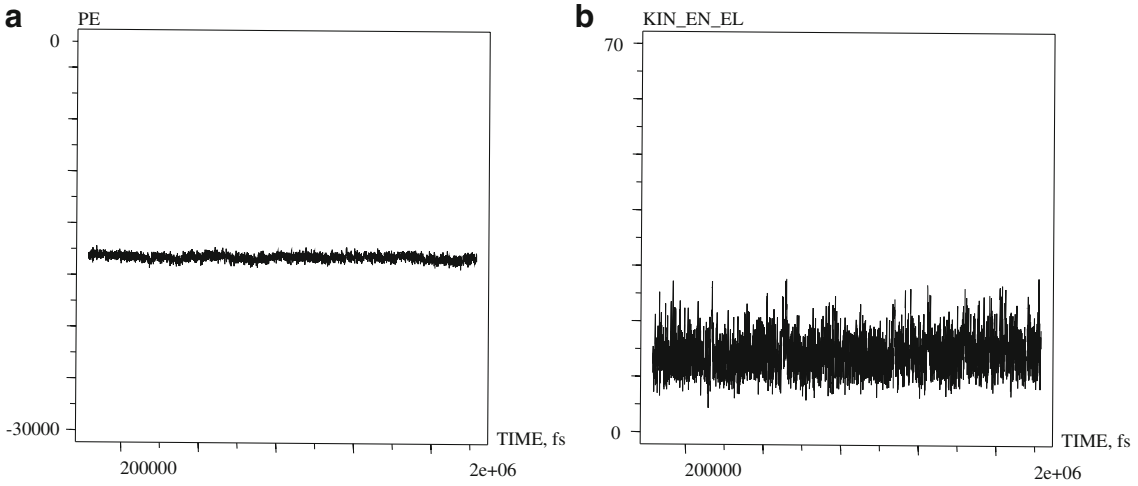


**Fig. 2** Examples of global system trajectory (DNA+ $e^-_{aq}$) and local thermodynamic ($e^-_{aq}$) parameters during 2 ns MD run: (**a**) Full system potential energy (PE, kcal mol$^{-1}$); (**b**) $e^-_{aq}$ kinetic energy. Abscissa in all plots is in femtoseconds

## Results

### Solvated electron – the model structure and hydrodynamics

Figure 3 shows the classic Kevan's 3D structure of the $e^-(H_2O)_6$ cluster as deduced from electron spin-echo experiments in glassy matrices at 77 K [14]. The model suggests that the electron is surrounded by six bond-oriented $H_2O$ molecules in an octahedral conformation, with the nearest hydrogen atoms located 2.1 Å from the structure centroid. From AM1 *semi*-empirical MO computations and Mulliken population analysis ($C_i$-symmetry), we obtained the following partial charges within the $e^-(H_2O)_6$ anionic cluster: 0.165 and 0.181 (in/out-ward pointing H-atoms, respectively) and -0.514 (O-atoms). This charge distribution results (in the gas phase) in a high electronegative potential of ≥ -100 kcal mol$^{-1}$ (4.35 eV) in the discrete regions coinciding with O-atoms VdW surfaces (magenta spheres in Fig. 3a), and evolves to an almost spherical electronegative surface at larger distances, e.g., - 40 kcal mol$^{-1}$ at ~10 Å (yellow sphere in Fig. 3a). In preparation for the molecular mechanics (MM) minimizations, hydration and molecular dynamics (MD), the Mulliken charges were assigned as formal charges to all $e^-(H_2O)_6$ atoms. For comparison, water atoms in the AMBER7_FF99 force field bear 0.331 (H) and –0.662 (O) formal charge, i.e., in the $e^-(H_2O)_6$ cluster, the extra negative charge resides partially on H-atoms and asymmetrically affects the charge distribution and hence the dipole momentum. When the same $e^-(H_2O)_6$ structure was submitted to MM minimization, solvation and again minimization (AMBER7_FF99 force field) we observed a somewhat smaller cavity dimension (r ~ 1.8 Å) as compared with the AM1-optimized structure. Apart from FF parameterization limitations, this type of geometry deviation in $e^-(H_2O)_6$ clusters is discussed in the literature, and most often is interpreted as distortions due to transitions from glassy matrices to the amorphous (liquid) state [3, 5]. Consistent with the range of the subsequently applied MM procedures, we kept the MM minimized structure as a working $e^-_{aq}$ model (distance constrained). During MD runs the $e^-(H_2O)_6$ geometry was always intact. As exemplified by a randomly taken MD trajectory snapshot shown in Fig. 3b, the $e^-(H_2O)_6$ cluster interacts with $H_2O$ molecules from the "second" shell of hydration (~1.5 Å thickness) comprised of 10–12 water molecules. These molecules are held close to $e^-(H_2O)_6$ by a network of interchangeable H-bonds and, in the absence of DNA, the halftime exchange rate with the bulk water is about 10 ps. Figure 3b presents two color-coded electronic map surfaces (electrostatic potential). One is for the $e^-(H_2O)_6$ cluster itself (grid-

**Table 1** Average system global thermodynamic and calculated hydrodynamic parameters of the $e^-_{aq}$ alone and in the presence of DNA

| *Data* | $e^-_{aq}$ alone | $e^-_{aq}$ -DNA |
|---|---|---|
| PE | −1926±119 | −1.7 x10$^4$±246 |
| KE | 1410±27 | 6660±50 |
| T | 255±5 | 250±2 |
| T-Local($e^-_{aq}$) | 260±41 | 263±64 |
| KE($e^-_{aq}$) | 14.7±5.4 | 14.1±3.4 |
| $R_{GYR}$($e^-_{aq}$) | 2.26±0.06 | 2.28±0.07 |
| $DEF_{ABS}$($e^-_{aq}$) | 3.02±0.58 | 3.13±0.45 |
| D($e^-_{aq}$)×10$^{-9}$ | 1.6±0.4* | 3.9±0.7 |

PE, System potential energy (kcal mol$^{-1}$); KE, Kinetic energy (kcal mol$^{-1}$), T, Temperature (°K); $RAD_{GYR}$, Radius of gyration (Å); $DEF_{ABS}$, Deformability (mass weighted RMS-deviation, Å); D($e^-_{aq}$), Diffusion coefficient (m$^2$ s$^{-1}$): (*) Reference data: experimental: 4.9×10$^{-9}$ (25°C); and extrapolated for 260 K, 1.4×10$^{-9}$ (-13°C) [38]; theoretical, 3.3×10$^{-9}$ (20°C) [4].

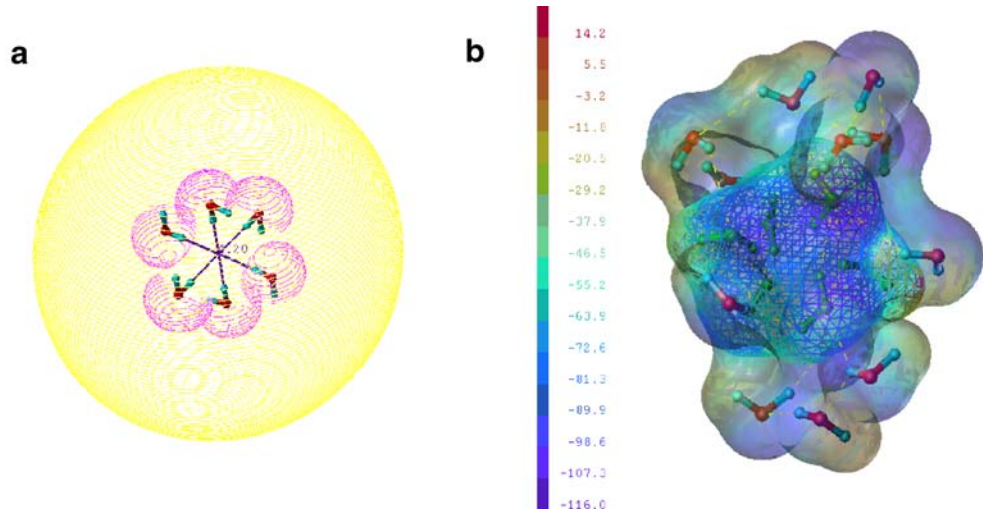


**Fig. 3** (**a**) The single water layer Kevan's cavity model of $e^-_{aq}$ after AM1-geometry optimization and Mulliken partial charge assignment. The distance between opposing inward H-atoms is 4.2 Å. In vacuum, the high negative electric potential encompasses the $e^-(H_2O)_6$ O-atoms VdW surfaces (magenta spheres; -100 kcal mol$^{-1}$) and becomes homogeneous at larger distances (yellow sphere; - 40 kcal mol$^{-1}$). (**b**) A random snapshot of $e^-_{aq}$ from 2 ns MD history file depicting only $e^-(H_2O)_6$ (green ball-and-stick) and twelve "second shell" transiently bound $H_2O$ molecules (colored by atom type). The electronic surfaces are colored by potential: $e^-(H_2O)_6$ (mesh, deep blue, highly negative); "second shell" (transparent contour, various colors); H-bonds (yellow); electrostatic potential color ramp (left, kcal mol$^{-1}$)

mesh), and the second one (transparent solid) encompasses the "second shell" $H_2O$ molecules within the 3.5 Å sphere (from the $e^-_{aq}$ center of mass). It is seen that the expanded negative $e^-_{aq}$ electrostatic field is weakened (as compared with the gas phase, Fig. 3a) and less homogenous, but still most of the "inner shell" VdW surface is highly negative (approx. -100 kcal mol$^{-1}$), while the "outer shell" shows both, highly negative fragments around O-atoms, and slightly positive spots (the highest of +1.3 kcal mol$^{-1}$) around outward pointing H-atoms. These dynamic features, as well as the relative residency time of the "second shell" water molecules and the deformability of the $e^-(H_2O)_6$ were found to be important parameters characterizing DNA - $e^-_{aq}$ interactive states. Hydrodynamic parameters, such as the mean absolute deformability ($DEF_{ABS}$) and the mean radius of gyration ($R_{GYR}$) during 2 ns MD runs of $e^-_{aq}$ in neat water, or in the presence of DNA with counter ions are listed in Table 1. The mean $R_{GYR}$ (~2.3 Å) and $DEF_{ABS}$ (~3.0 Å) remain almost unchanged in the presence of DNA. This is interpreted to be a consequence of the relatively rare interactions with DNA, i.e., most of the time $e^-_{aq}$ moves surrounded by solvent water only, and the average structure is unperturbed (for details, see below). Assuming that the Brownian motion of the $e^-(H_2O)_6$ cluster follows the Einstein-Smoluchowski law and from short linear selections in the XYZ_Abs plots, i.e., omitting close to DNA positions when it was present (Fig. 4a), we calculated the diffusion coefficients, $D(e^-_{aq})$. The resulting average $D(e^-_{aq})$ for the electron alone is $(1.6\pm0.4)\times10^{-9}$ m$^2$ s$^{-1}$ and $(3.9\pm0.7)\times10^{-9}$ m$^2$ s$^{-1}$, in the presence of DNA (Table 1). The obtained values are close and fall within the range of the reported experimental [38] and theoretical estimates [4]. Although, in the presence of DNA the $e^-(H_2O)_6$ movement was more abrupt, it could be approximated as linear and monotonous during at least 10–20 ps (when not retained by DNA, Fig. 4b). However, if longer than 20 ps trajectory steps were used in calculations, $D(e^-_{aq})$ values as high as $\sim8\times10^{-9}$ m$^2$ s$^{-1}$ were estimated. The reasons for this acceleration are not clear, and could be due to inherent Brownian diffusion problems (definition and averaging), as well as to specific physical interactions (long range) with solvent/solute.

## Solvated electron residence sites around DNA: mobility and dynamics of water exchange

The $e^-_{aq}$ movement during MD runs is represented by the 2D-trajectory of the absolute displacement (XYZ_Abs) of the $e^-_{aq}$ center of mass (Fig. 4). The trajectory demonstrates an oscillation pattern: the electron traverses the space determined by the PBC, mostly in parallel to the z-axis of the compete DNA turn; from the O3′-end of the non-brominated strand up to its upper O5′-end; moves back close to the starting point (O3′-end), then a similar path is repeated. Sybyl computational and interactive-graphics tools allowed us to track the entire $e^-(H_2O)_6$ motion during the 2 ns simulation. From the radial-distance functions, such as XYZ_Abs, or trajectories, defined as distance between $e^-(H_2O)_6$ and any nucleotide, it was found that the electron samples the PBC box and the DNA interface in all directions, but shows preference to locate in the space facing the major groove. Longer (>20 ps) linear segments

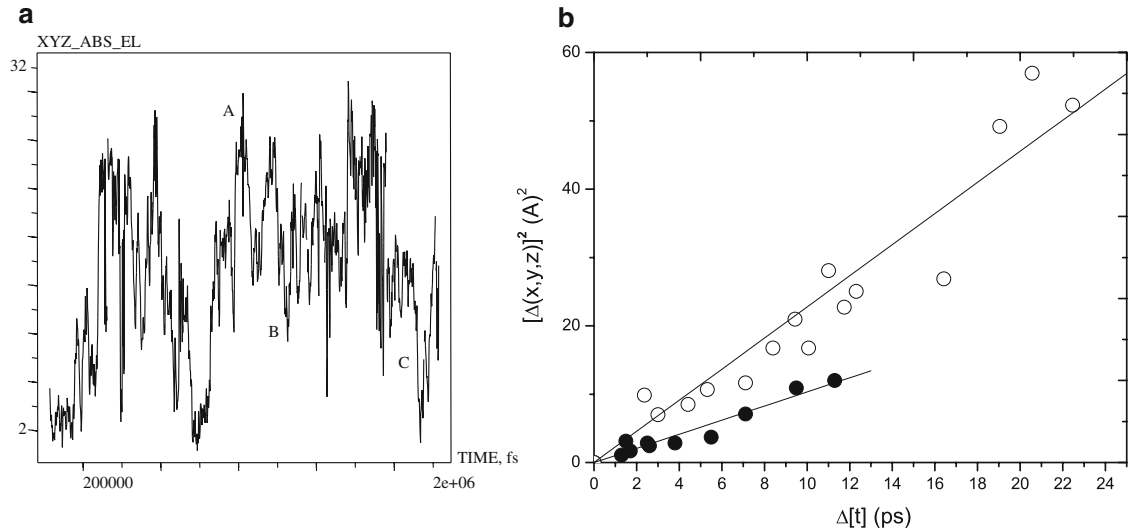


**Fig. 4** (**a**) Absolute displacement of $e^-_{aq}$ center of mass (XYZ_Abs) during 2 ns MD run in the presence of DNA and counterions. Reference $e^-_{aq}$ coordinates: beginning of the production run (see Fig. 1); (**b**) $[\Delta(X,Y,Z)]^2$ *vs*. Δt plots for $e^-_{aq}$ alone (filled symbols) and in the presences of DNA (open symbols). Data were extracted from the corresponding XYZ_ABS trajectories and used for the calculation of D($e^-_{aq}$) presented in Table 1. For the meaning A,B,C labels see Fig. 5

in Fig. 4a represent unperturbed longitudinal (e.g., along the major groove cleft), or transversal (from one strand toward the other) $e^-_{aq}$ motion in respect to DNA. Different directions of the unperturbed motion of the electron are illustrated by the 3D $e^-_{aq}$ tracks during ~30 ps shown in Fig. 5, marked A,B,C. Each of them corresponds to the three linear segments, marked in the XYZ_Abs plot (Fig. 4a). Thus, $e^-_{aq}$ was found passing over/below the DNA ends (A) and transiently retained there, or in a few occasions, not far from the minor groove (B). These sites, however are not included in the following analyses because: i) the interaction with DNA ends was deemed artificial (presuming in reality that the DNA duplex is infinite) and; ii) $e^-_{aq}$ is not known to discharge by CT transfer to DNA backbone atoms, in contrast to "dry", low energy electrons. The most usual direction of the $e^-_{aq}$ motion was that depicted in track (C), which is along the major DNA groove. Likewise, the sites of close interactions with DNA nucleobases were most often found in this region.

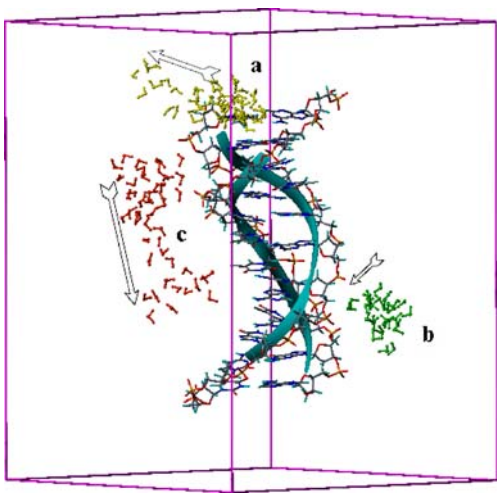


**Fig. 5** Superimposed on the averaged (2 ns) DNA structure series of electron positions (snapshots, Δt=5 ps) of unperturbed $e^-_{aq}$ motion, extracted from three linear XYZ_Abs segments of 25–35 ps lengths, and marked A,B,C in Fig. 4a. (**a**) Presents positions when $e^-_{aq}$ was initially immobilized at the upper DNA end and released; (**b**) Shows transversal to DNA (perpendicular to Z-axis) motion, in a direction from the non-brominated strand to the brominated (minor groove side); (**c**) Presents $e^-_{aq}$ 3D-track lateral to the Z-axis and facing the major groove. Balls and sticks: electron in yellow (**a**), green (**b**) and, red-range (**c**); DNA backbone, cyan (shaded ribbon). Directions of predominant motion are indicated by arrows

Using the row-selection tools of the Sybyl "dynamics-table" program we have identified configuration states of short distances between any $e^-(H_2O)_6$ outward hydrogen and solvent-exposed nucleobase (NB) heteroatoms. Figure 6 presents a integrated view of superimposed MD snapshots of configuration states selected by the rule, distance $|e^-_{aq}$(H)–NB atom|<5 Å. The clustered 62 $e^-_{aq}$ positions usually belong to sequential states of 0.5 ps each, representing a preferred residence space (site). In only nine configurations the DNA-$e^-_{aq}$ distance was <4 Å. When intermediate $e^-_{aq}$ re-orientation configurations were included (e.g., by selecting larger cut-off distance), in some of these sites the $e^-_{aq}$ was retained as long as 50–60 ps, but the individual states of the closest approach persisted no longer than a few ps (Table 2).

In the 2 ns MD time frame, the occupancy of the close to DNA space is 1.55% at <5 Å and only ~0.2% at <4 Å cut-off distance. The residence sites of the closest approach to DNA shown in Fig. 6 are numbered consecutively with the elapse of MD run time. Rather surprisingly, the results

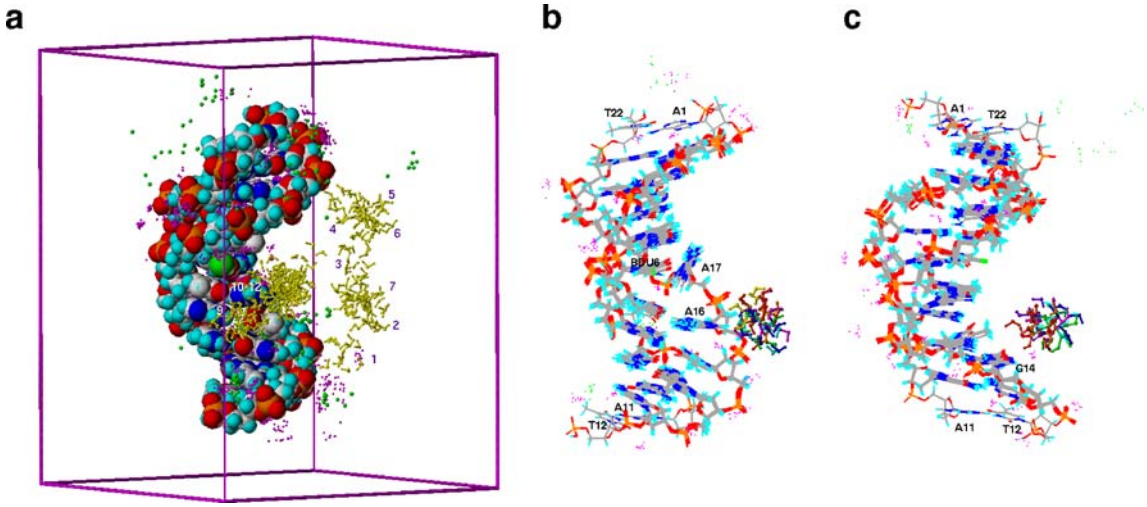


**Fig. 6** (**a**) Configuration states (superimposed snapshots) of the closest approach of $e^-_{aq}$ to DNA selected by the rule: $|e^-_{aq}(H)$ – NB atom|<5 Å (total of 57 dynamic states); DNA (space fill) averaged structure from 2 ns MD; $e^-_{aq}$ (yellow, ball-and-stick); Br-atom (green VdW sphere); $Na^+$ ions (magenta balls); $Cl^-$ ions (green balls); hydration water, not shown; (**b**) Site-2, superimposed 9 actual configurations (Table 2), note the large opening between A16 and A17 due to the close $e^-_{aq}$ (various colors, ball-and-stick); (**c**) Site-9, characterized by a relatively unperturbed DNA structure

present a non-random distribution along DNA; $e^-_{aq}$ tends to move in and to revisit only certain sites close to DNA. As can be seen from Fig. 6 and Table 2, the close contact sites are within the vicinity of four nucleotides: G14, T15, A16 and A17. Although A17 is paired with BU6, the latter was not approached by the electron (i.e. $e^-_{aq}$ shows a preference for the non-brominated strand only). Figure 6b illustrates the close contact site-2, when $e^-_{aq}$ interacts with A16 from the A17 side, and the later is strongly disoriented. In Fig. 6c $e^-_{aq}$ interacts with G14 (site-9) and the DNA structure is intact, as in other cases when the electron approaches the G·C base pair. The shortest contact distance is determined by the variations in the dynamic packing of hydration water shells, both the water molecules tightly bound to DNA (~5–6 $H_2O$ per base in the major groove), and the transient second water-shell around the $e^-(H_2O)_6$ cluster, from which 10–12 were steadily H-bonded to the $e^-(H_2O)_6$ core in any arbitrary MD snapshot (see Fig. 3b). At the sites of closest contact, the water layers separating $e^-(H_2O)_6$ from DNA varied from one to two (Table 2), which means that in some configurations DNA and $e^-(H_2O)_6$ shared the same single water shell (see below). In most cases, shared $H_2O$ molecules formed a one-to-three step H-bonding network connecting $e^-(H_2O)_6$ with DNA and in some sites a single molecule participated in bifurcated H-bonds. Figure 7 presents zoomed 3D-views of three individual configurations of close DNA - $e^-(H_2O)_6$ contacts. Typically, the shortest distances between $e^-(H_2O)_6$ and NB-atoms were 3.7 and 4.9 Å, but a single site was found where the electron moved close to DNA in sequential steps reaching a

**Table 2** Sites of close contact between $e^-_{aq}$ and DNA as selected by the rule $|e^-_{aq}(H)$– NB atom|<5 Å (see Fig. 6)

| Site ID | Elapsed time, ps | Closest DNA atom | Shortest distance, Å | Population (number of conf. states) | Lifetime ps | Water structure | |
|---|---|---|---|---|---|---|---|
| | | | | | | $H_2O$ layers | H-bridged[2)] |
| 1 | 0.26 | (T15)C5M | 3.83 | 3 | 1.5 | 2 | 0 |
| 2 | 0.27 | (A16)N7 | 2.73 | 9 | 4.5 | 0 | direct H-bond |
| 3 | 0.28 | (A17)N6 | 3.94 | 3 | 1.5 | 2 | $2\times5H_2O$ |
| 4 | 0.36 | (A17)N6 | 3.74 | 2 | 1.0 | 1 | $2\times3H_2O$ |
| 5 | 0.37 | (A17)N7 | 4.95 | 1 | 0.5 | 1 | $1\times1H_2O$ |
| 6 | 0.38 | (A17)N7 | 3.74 | 8 | 4.0 | 1 | $1\times2H_2O$ |
| 7 | 0.47 | (A16)N6 | 4.79 | 1 | 0.5 | 2 | $1\times2H_2O$ |
| 8 | 1.36 | (A16)N6 | 3.82 | 1 | 0.5 | 1 | $2\times2H_2O$ |
| 9 | 1.47 | (G14)O6 | 3.61 | 14[1)] | 7.0 | 1 | $3\times3H_2O$ |
| 10 | 1.51 | (G14)O6 | 4.97 | 1 | 0.5 | 2 | $2\times2H_2O$ |
| 11 | 1.85 | (A16)N7 | 4.03 | 8 | 4.0 | 1 | $1\times1H_2O$[3)] |
| **12** | 1.89 | (T15)C5M | 3.37 | 12 | 6.0 | 1 | 0 |

[1)] Includes five additional (intermediate) configuration states.
[2)] Number of H-bridges between a nucleotide and $e^-_{aq}$ and number of $H_2O$ molecules involved.
[3)] The contact atom is (A16) O2P. For each site the last column refers to the state of the closest distance.

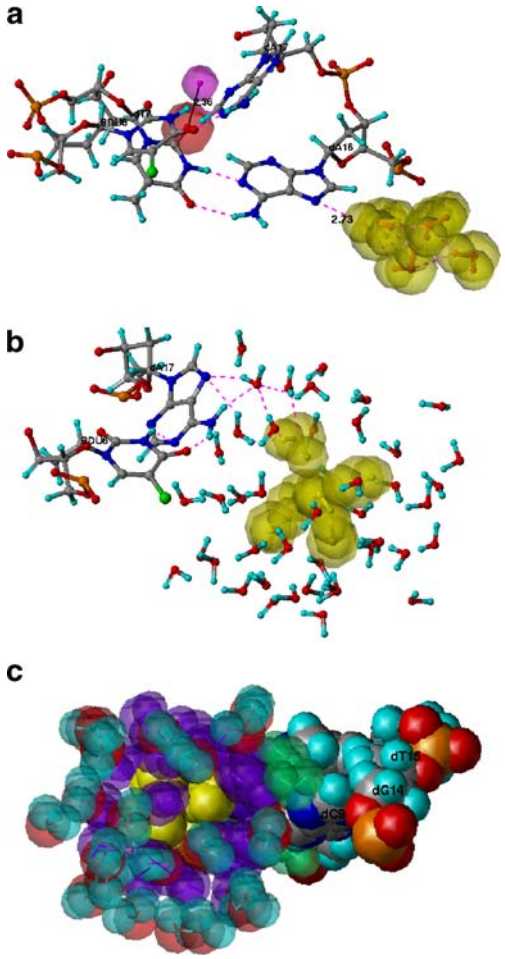


**Fig. 7** (**a**) The only configuration of a close approach of $e^-_{aq}$ to DNA where a direct H-bonding between the hydrated $e^-_{aq}$ and a NB-atom (N7 of A16) was found. H-bonds (magenta); distances in Å; $e^-_{aq}$ as VdW surface (yellow). The BU6·A17 and T7·A16 pairs are correctly H-bonded, but both exhibit high stagger and buckle, and A16 and A17 are loosely stacked; the VdW sphere (magenta) represents a $Na^+$ ion found to penetrate deep into the double helix from the opposite (minor groove) side and located at 2.36 Å from O2(T7) (red sphere); (**b**) Example of an intricate H-bonding pattern formed between $e^-_{aq}$, hydration water and NB in a close approach configuration (site-6; in this case 4 water molecules are involved in a two step H-bond network); and (**c**) Structure of a tightly formed contact state (VdW spheres), involving a single shared layer of tightly packed water (purple, transparent): $e^-_{aq}$ (yellow, solid), A8·T15 and C9·G14 base stack (atom color, solid), DNA only bound water (green, transparent), and bulk water (atom-type color, transparent,)

shorter distance. This contact (site 2, also shown in Fig. 6, Table 2) is unique because the electron is in direct (no water bridges) H-bonding with N7(A16) and the distance $|e^-_{aq}(H) - N7(A16)|$ could be as short as 2.73 Å. The electron resides in this area about 9 ps, showing small fluctuations and occasionally approaches the amino-hydrogen atom, H61 N6 (A16) atom, but without forming a direct contact. Later it relocates away from this position. At the time of the closest approach, when the electron is directly H-bonded to N7, the $e^-(H_2O)_6$ cluster is elongated since one $H_2O$ molecule is strongly attracted to N7 and the DEF_Abs($e^-_{aq}$)= 3.64, which is about 20% higher than the average for this MD run (Table 1). However, the radius of gyration is not significantly affected (=2.38 Å). Importantly, the T7·A16 H-bonding was not disturbed, and the two DNA strands remained correctly paired. Nevertheless, when the electron was visiting this area later, specific conformational perturbations within the central DNA triplet sequence were observed, involving significant dislocation of the $Na^+$ counterions associated with these nucleotides and side-chain displacement. In general, greater DNA-duplex distortions were observed within the central part of the DNA duplex facing the solvent space where the electron resided for longer time, concomitant with deep penetration of opposing $Na^+$ ions, as shown in Fig. 7a. The next two configurational states shown in Fig. 7b,c (sites 3 and 9) illustrate the different arrangement of the water layers (H-bonding and packing) and are representative for the rest of the close approach sites (except site 2). From the dynamics history file it was possible to track the build up and decay of the water layers around $e^-(H_2O)_6$ and DNA. Most often a water molecule was recruited from the bulk solvent into the "second" $e^-(H_2O)_6$ shell for about 3–4 ps. To illustrate the dynamics of this process we present an arbitrarily chosen 25 ps trajectory XYZ_Abs segment of a water molecule (ID O7547) which was initially ~5Å apart from the $e^-_{aq}$ (the electron was in the vicinity of site-6) and was recruited into the "second" $e^-(H_2O)_6$ shell for about 4 ps at the side furthest from the DNA (Fig. 8a). During the remaining 12 ps after being released, it traveled away ~20 Å, which illustrates the typical unrestricted motion of solvent water. Water exchange between DNA and $e^-_{aq}$ occurred in two directions. Often a water molecule was first engaged by $e^-_{aq}$ and if meanwhile it approached DNA, this water could become H-bonded to NB atoms and remained in this tightly bound, "shared water-layer" state for maximum 7–8 ps. The opposite exchange from the tightly DNA-bound water shell to $e^-_{aq}$ "second shell" was rarer. Figure 8b demonstrates the dynamics of such a process. The trajectory of the water molecule (ID O3942) which is shown in the transient state Fig. 7b, as forming four H-bonds with A17N7, A17N6H62 and two "second shell" $e^-_{aq}$ water molecules was traced during the same 25 ps MD segment as above. Initially it was H-bonded to A18. With the $e^-_{aq}$ approach to A17 (site-6) this water was shortly recruited in the shared between DNA and $e^-(H_2O)_6$ hydration layer and released, but still remained in the DNA hydration shell (moving along DNA), and thus more restricted (compared to bulk water). The conjugated motion of $e^-_{aq}$ during the same period is presented by the XYZ_Abs trajectory of its center of mass (Fig. 8c) and by the trajectory of the shortest inter-DNA/$e^-_{aq}$ distance (Fig. 8d). An important observation is that during the time when $e^-_{aq}$ resided close to DNA (arrows in

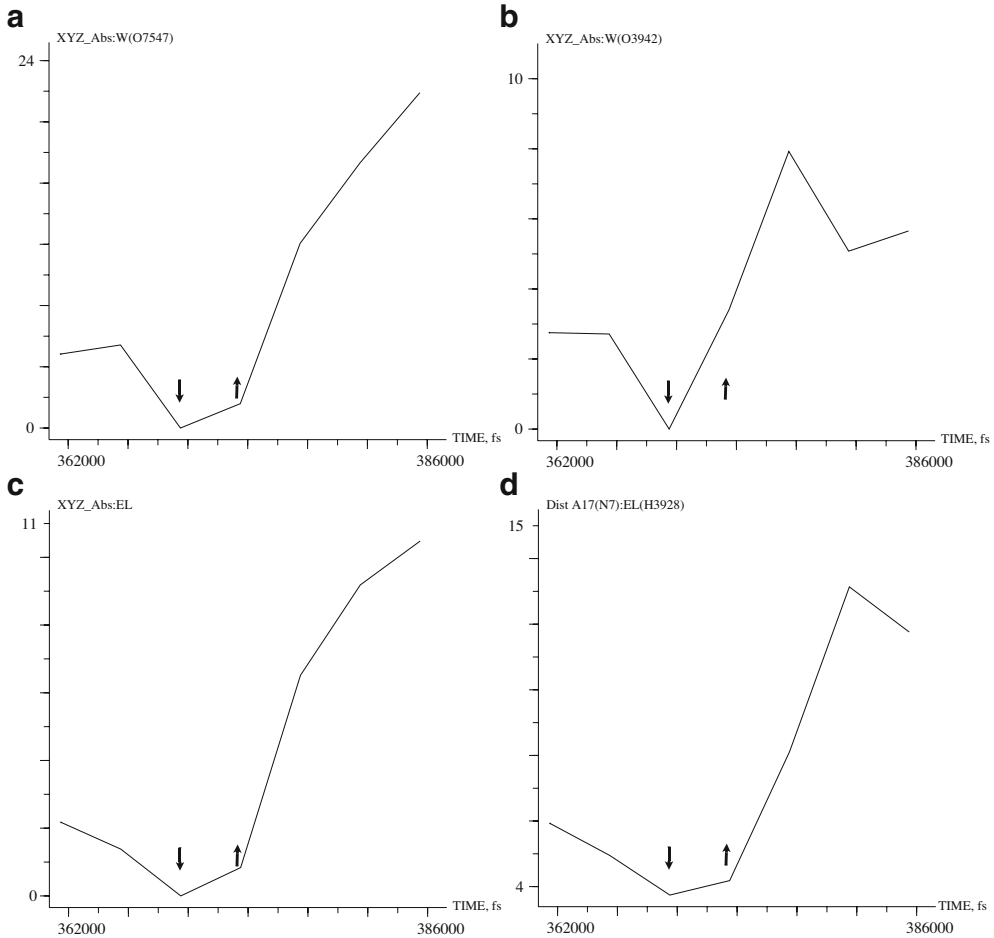


**Fig. 8** Electron motion and water exchange in a short 25 ps period, during which $e^-_{aq}$ approaches the N7(A17) atom (site-6, Fig. 7b) and later disengages. (**a**) Absolute displacement of a water molecule which was recruited in the "second" $e^-_{aq}$ hydration shell at the opposite to the DNA $e^-_{aq}$ side, and later released in the bulk solvent. (**b**) Absolute displacement of a water molecule, which at the beginning of the period was part of the DNA hydration shell, interacting first with A18 (initial plateau), later attracted by A17, recruited in the shared DNA- $e^-_{aq}$ shell (Fig. 7b, and subsequently relocated in the vicinity of A16; (**c**) Absolute displacement of the $e^-_{aq}$ center of mass (XYZ_Abs) during the same MD segment and; (**d**) Distance trajectory between two atoms N7(A17)-H3928 ($e^-_{aq}$) which were in closest approach when the electron was retained by DNA in site-6. Distances in Å, ordinate (time) in fmts, averaged spline-lines, reference coordinates (zero) in all XYZ_Abs plots are of the configuration of minimum DNA- $e^-_{aq}$ distance (Table 2), arrows mark the approximate duration of $e^-_{aq}$ immobilization at this site (residence time of *ca.* 4 ps)

Fig. 8), its immobilization was mirrored by immobilization of surrounding ("second" shell) water. The existence of at least two distinct classes of water, apart from the transient immobilization by $e^-_{aq}$ is demonstrated by the remaining parts of the trajectory plots. The bulk water traverses at least 20 Å during the 11 ps after $e^-_{aq}$ leaves DNA, while the DNA-bound (structured) water, as the $e^-_{aq}$ itself are displaced by no more than 8–9 Å.

## DNA dynamic conformations vs. system dynamic configurations

*General view* MD simulations of hydrated DNA in the presence of counterions and the $e^-(H_2O)_6$ cluster revealed conformational peculiarities, which did not exist when MD was performed in the absence of $e^-(H_2O)_6$. In the most general terms, the outcome is that the bulky $e^-(H_2O)_6$ anion interacts both, sterically (short range) and electrostatically (long range, plus H-bonding) with various partners (nucleotides, water and counterions) and evokes significant perturbations. Some of the most remarkable deviations from the canonical WC DNA double helix structure and counterion rearrangements are conferred below. An integral view of DNA structural deviations is shown in Fig. 9, where superimposed DNA helices include initial and averaged (from 2 ns MD) structures and two transient (snap-shot) dynamic DNA structures. The later were selected to represent configuration states of close $e^-_{aq}$ approach to DNA, as discussed in the previous section. Although depicted as single dynamic states, they signify the most populated $e^-_{aq}$ residence sites in the vicinity of DNA. It can be seen that the DNA backbone (in this case, the C1′

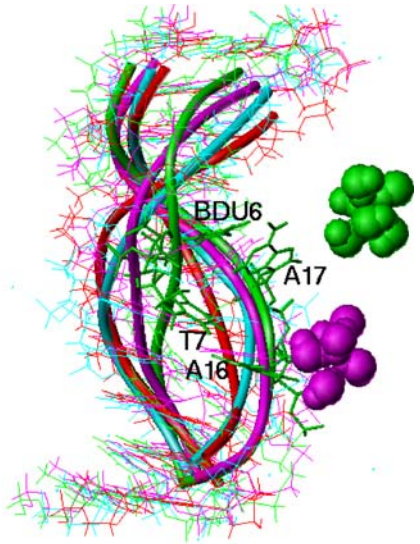


**Fig. 9** DNA deformations during 2 ns MD run. Superimposed are the starting (cyan) and averaged (red) structures, as well as two snapshots representing configurations of close $e^-_{aq}$ approach (green and magenta). DNA backbone (tubes); $e^-_{aq}$ (VdW space fill). Note the large major groove gap between BU6·A17 and T7·A16 (green, caped sticks). The most significant is the displacement of A17. However, starting and averaged DNA structures are close to one another

atoms interconnecting line) is notably distorted. On some occasions, bases close to $e^-_{aq}$ are pulled into the major groove and become highly exposed to the solvent. In order to sterically accommodate base displacement but to also preserve nearest neighbor base-pairing, the backbone becomes distorted, as shown. The displacement of $Na^+$ counterions, initially located near the shallow cleft of the minor groove (close to the phosphate groups), appears to play a major role in the generation and stabilization of the distorted DNA conformational states. In general, the minor groove widens when the electron is located within the vicinity of the major groove and the non-brominated strand is pulled toward the electron, such that both strands are affected. The distortions tend to repair with elapsed time as seen by the near overlap of the average and initial structures.

*$Na^+$ ion translocation* Sodium counterions XYZ_Abs plots, distance trajectories and averaged structure superimpositions indicated that while condensed and usually well localized around the DNA, $Na^+$ counterions still maintained a highly dynamic character and during 2 ns could undergo significant displacement (>10 Å). For different Na-ions in the minor groove, the typical (dynamically defined) residence time was about 100 ps, but could be as long as 300 ps. The long lived sites existed when a particular $Na^+$ ion was found trapped deep within the minor grove and was interacting not only with phosphate group oxygen atoms, but with NB atoms, as well (see Fig. 7a). In these configuration states the DNA helix was opened and the C1′-C1′ interstrand distances increased by at least 0.5 Å. About seven $Na^+$ counterions tended to penetrate deeper in the minor groove, all of them located in the vicinity of G14, T15, A16 and A17, *i.e.*, the nucleotides closely approached by the electron (Fig. 6 and Table 2). The molecular forces responsible for this deep minor groove penetration of $Na^+$ were not studied in detail, but they likely involve electrostatic attraction by $e^-_{aq}$ since such configurations were initiated after the electron approached the DNA major groove directly opposing a particular $Na^+$ ion. With the elapse of the MD simulation time the most of the specific sites of deep $Na^+$ localization were repaired and the counterions rearranged.

*DNA structure and dynamics of the canonical base-pairing* As noted above, the DNA dynamic structure was sensitive to the presence of $e^-_{aq}$. DNA MD with different force fields results in deviations from typical A/B DNA structures, especially for AT tract DNA's, as in the present case (five subsequent AT pairs in the middle of the duplex) [39]. Such B-DNA segments tend to bend, have shallower minor grove and higher base pair tilt, as in A-DNA. Indeed, in the absence of $e^-_{aq}$ the studied DNA structure showed higher base inclination in the AT tract (up to 14°), as well as other deviations of intra- (propeller/buckle) and inter-base (roll/tilt) parameters, rendering the structure as intermediate A/B DNA (details will be presented elsewhere). For instance, the intra-strand P-P distances in the AT region tended to decrease from 7.0 Å to about 6.2 Å. These tendencies were retained in the presence of $e^-_{aq}$. However, the extreme base pair deviations (mostly transient) when the $e^-_{aq}$ approached given DNA sites, e.g., interacting bases pulled out into the major groove could not be fitted to any typical DNA type. To illustrate the extent of this phenomenon, we present comparative data depicting distortions in the WC H-bonding pattern. Table 3 lists selected interstrand base-pairing (H-bonding) distances in DNA with and without presence of $e^-_{aq}$. In the presence of $e^-_{aq}$, the WC H-bonding was largely preserved within the end base pairs, and the central BU6·A17 base pair. However, the flaking base pair, T7·A16 showed proper H-bonding for only about 8% of the total time, and this tendency was true for A8·T15 and C9·G14 pairs, all involving nucleotides approached by $e^-_{aq}$.

Obviously, this disruption results from the close presence of $e^-_{aq}$. The A16 base was most often found displaced from its regular position and flipped-out in the major groove (Figs. 6b and 9). In addition, $Na^+$ counterions which interact with the T7·A16 and A8·T15 base pairs show the deepest minor groove penetration and the longest residence times, as presented in Fig. 7a. It is noteworthy that, although the unusual dynamic states were transient and tended to repair, the system clearly kept a

**Table 3** Canonical DNA structure deviations during 2 ns MD in the presence, or not of $e^-_{aq}$. Watson-Crick H-bonding: mean distance and incidence (% of 4000 MD frames)

| Inter-base contact atoms | DNA + $e^-_{aq}$ | | | DNA | | |
|---|---|---|---|---|---|---|
| | Distance (Å) | H-bonded[1)] | WC paired[2)] | Distance (Å) | H-bonded[1)] | WC paired[2)] |
| (G3)N2H2·O2(C20) | 2.0±0.2 | 98 | 95 | 2.0±0.2 | 97 | 97 |
| (G3)N1H·N3(C20) | 2.0±0.3 | 95 | | 1.9±0.1 | 100 | |
| (A4)N6H62·O4(T19) | 3.2±1.2 | 43 | 40 | 2.4±0.5 | 76 | 76 |
| (A4)N1·HN3(T19) | 2.8±0.6 | 42 | | 2.3±0.3 | 81 | |
| (T5)O4·H62N6(A18) | 2.7±0.8 | 51 | 50 | 2.4±0.4 | 65 | 65 |
| (T5)N3H·N1(A18) | 2.2±0.4 | 77 | | 2.2±0.1 | 98 | |
| (BU6)O4·H62N6(A17) | 2.1±0.1 | 87 | 84 | 2.1±0.2 | 99 | 98 |
| (BU6)N3H·N1(A17) | 2.0±0.1 | 85 | | 2.0±0.1 | 98 | |
| (T7)O4·H62N6(A16) | 4.3±0.9 | 8 | 8 | 2.4±0.4 | 63 | 57 |
| (T7)N3H·N1(A16) | 2.9±0.6 | 27 | | 2.6±0.5 | 58 | |
| (A8)N6H62·O4(T15) | 3.7±1.2 | 25 | 5 | 2.6±0.5 | 68 | 54 |
| (A8)N1·HN3(T15) | 3.6±0.6 | 5 | | 2.9±0.7 | 54 | |
| (C9)O2·H2N2(G14) | 2.6±0.4 | 47 | 17 | 2.2±0.2 | 96 | 89 |
| (C9)N3·HN1(G14) | 3.4±0.7 | 18 | | 2.3±0.3 | 89 | |
| (G10)N2H22·O2(C13) | 2.0±0.1 | 100 | 73 | 2.0±0.1 | 100 | 96 |
| (G10)N1H·N3(C13) | 2.3±0.3 | 74 | | 2.3±0.2 | 96 | |

[1)] Single H-bonding defined by donor-acceptor inter-atomic distance≤2.5 Å and proper angle;
[2)] Two simultaneous WC H-bonds between partner bases (% of total MD configuration states).

"memory" of the configurations of close $e^-_{aq}$ approaches. Interestingly, nucleobases, even when displaced, rarely formed atypical cross-strand interatomic contacts, as in wobble DNA [27].

## Discussion

*Overview* The MD simulations of BUdR-substituted DNA in the presence of a solvated electron, modeled as a cavity-localized $e^-(H_2O)_6$ ionic cluster, present insights into the system dynamics, including how $e^-_{aq}$ approaches the DNA duplex and to a what extent the close approach perturbs the DNA dynamic structure. The recurring stable output from the production MD runs is encouraging and assures that the method is appropriate for this application. Although the PME method was not used the energy fluctuations were acceptably small (Fig. 2, Table 1) without any noticed mirror-image interactions, which indicates that the applied FF parameters were correctly chosen; the NB-cutoff with 1–4 electrostatics scaling and the more frequent NB-update [27, 32, 33]. Notably for the isobaric ensemble; system total, kinetic and potential energies were constant throughout the MD runs, as well as those of the electron, counter-ions and solvent. The accuracy of our $e^-_{aq}$ model and MD simulations is also supported by the correct assessment of the mean diffusion coefficient, $D(e^-_{aq}, 260\ K)=(1.6\pm0.4)\times10^{-9}\ m^2\ s^{-1}$, which for the electron falls in the range of the reported theoretical and experimental estimates (Table 1) [4, 38]. Interestingly, in their original paper Essmann et al. [31] found that various treatment of the dispersion interactions (PME, Ewald, or truncate) did not significantly affect either water density, or the diffusion constant. Our simulations predict that in the presence of DNA, apart from being more disruptive, the Brownian $e^-_{aq}$ movement in the bulk water on average is somewhat accelerated when compared with the reported value, extrapolated for 250 K [38] (excluding immobilization when sites close to DNA were occupied). Thus, our findings support the earlier conclusions of relatively high mobility of excess electrons in water, as compared with classical anions ($Br^-$ $Cl^-$, etc.) and based on the Nernst-Einstein evaluation, without necessarily invoking quantum mechanical transport mechanisms [40].

*Adherence to the mechanisms of electron transfer (ET) to DNA* Notwithstanding recent advances in the elucidation of the structure and optical properties of excess electrons in water and excess electron transfer along DNA [17], little is known about the mechanistic details of primary $e^-_{aq}$ reduction of DNA. General considerations on the applicability of extended Marcus CT theory [41] and Savéant theory of dissociative ET [42] for hydrated electron-mediated ET have been discussed in the case of small molecules only. The trend for the reducibility of nucleotides (experimental $E^o$red) in solution [1, 22] follows the order of electron affinities (EA) U~T>C>A>G as corroborated also by theoretical methods [23]. Thus T and C act as "stepping stones" for the hopping-type electron motion in DNA [17, 18]. Experimental reducing potentials (E°red) in

DNA are not available, but reliable theoretical computations indicate significant changes of EA and IP due to specific hydration patterns, base stacking and pairing [43]. A recent report points out that BUdR is likely to be ~40 mV easier to reduce than thymidine [44], however an accurate E°red (BUdR) in DNA is unknown. Excluding possible "tunneling" ET to DNA, which could take place at large distances (>10 Å), our MD study presents insights into the modalities of "contact" $e^-_{aq}$ interaction with DNA. In the present molecular modeling approach all system components obey Newtonian mechanics rules and thus microscopic (quantum and chemical) interactions can not be judged, i.e., the ET process as such, for which higher order quantum mechanical simulations must be performed. The classical presumption for ET to occur is that $e^-(H_2O)_6$ and DNA must be close to each other, yet there might be system configurations which do not allow $e^-_{aq}$ to "discharge" (e.g., improper ΔE°red). Such intrinsic properties can be further studied by applying quantum mechanical ab initio (e.g., DFT) computations on selected system configuration states (MD snapshots), or by applying thermodynamic rules (e.g., Marcus-Savéant theory) [41, 42]. From the classical mechanics perspective, instances when ET is completed can not be determined; thus, the interpretation of the present MD results is intuitively physical (statistical) and is based on the assumption that molecular encounter frequency and/or residence time of $e^-_{aq}$ determine the probability of ET. The current study represents an initial approximation to the problem of identification of the interaction modes of $e^-_{aq}$ and DNA.

*Relationship to the BUdR mediated damage in DNA* It appears that there are preferred $e^-(H_2O)_6$ residence sites around the DNA major groove, which are likely to depend also on the local DNA-counterions-water configuration states, exerting specific steric and electrostatic field effects. Thus, it was found that $e^-_{aq}$ tends to localize near only four NB, and most importantly does not closely approach BUdR incorporated in the DNA. The closest distance from O4 (BU6) to $e^-(H_2O)_6$ was 6.1 Å, but at this dynamic configuration the nearest contact atom was N6(A17), r= 3.9 Å. These findings agree with our experimental BUdR radiosensitization studies [24–26], showing that completely double stranded BUdR-DNA is much less prone than single stranded (or wobble DNA) to radiation damage (strand breaks and interstrand crosslinks). The results support a presumption that the likely acceptors of the excess electron from the bulk water would be T15 (but not BUdR), or A16 and A17 (albeit at a lower efficiency due to the moderate-to-low EA(ade)). This implies that to achieve BUdR reduction and dissociation, intra-DNA ET must take place. Since in this particular sequence the two T are proximal, the ET direction must be towards BU.

*Characteristics of the $e^-_{aq}$ – DNA interaction sites, DNA structure perturbation and water exchange* The structure, dynamics and build up of the water layer(s) between $e^-_{aq}$ and DNA might be important in the context of different CT theories of $e^-_{aq}$ interaction with DNA, e.g., continuum *vs.* discrete (stepwise) mechanism. Our results show that the sites of closest $e^-_{aq}$ approach to DNA may involve none, one, or two intermediate water layers (Table 2). The layers may also differ by the type of H-bonding network connecting the $e^-(H_2O)_6$ cluster with NB-atoms (N and O). No bridging H-bonds were observed in two occasions: i) when $e^-_{aq}$ was localized in the vicinity of C5 M(T15); and ii) when $e^-(H_2O)_6$ was directly H-bonded to N7(A16). The MD simulations also allowed us to trace the dynamic mobility of particular water molecules recruited in the "second" $H_2O$ shell of $e^-(H_2O)_6$, DNA, or both (Fig. 8). Analyses, which will be detailed elsewhere, showed differently structured water shells close to polar/non-polar NB groups and asymmetric water exchange with the $e^-_{aq}$ "second" shell, in general resembling water characteristics in other heterogeneous (protein) systems [45]. Further thermodynamic and/or quantum mechanical analyses will be required to determine at which of the above configurations the $e^-_{aq}$ capture by DNA is more plausible. Since $e^-_{aq}$ is an outer sphere donor and the ET and $S_N2$ ($S_{RN}1$) are the two extremes of the continuous mechanistic spectrum, it will be interesting to compute the global electronegativity, hardness and local softness [46], based on the condensed Fukui-functions analysis [47] and to predict DNA sites (atoms) of preferred $e^-_{aq}$ attachment. Finally, this work shows that the $^-(H_2O)_6$ anion cluster, when closely approaching DNA is capable of distorting the canonical (WC) duplex structure. These findings might also be important when DNA interacts with other bulky anions in solution. Presently, it is unclear to what extent the deviations are specific to the AT-rich DNA sequence studied [48]. Our (BUdR·A)-DNA structure simulations reaffirm the role of the partially positively charged T-methyl group in the 5′-ApT-3′ stacking/restriction (cation/π-interactions), implicated in the limitation of base mobility and thus, DNA bending at AT sites [49]. The most direct evidence is the largely preserved A·BU WC H-bonding (as compared to A·T), both in the absence and presence of $e^-_{aq}$ (Table 3).

## Conclusions

1) The described Newtonian MD simulations provide an insight into $e^-_{aq}$ motion and interactions with DNA, including identification of the sites of closest approach to DNA; 2) The results indicate specific $e^-_{aq}$ localization

preferences around DNA; 3) In general, the interactions of the $e^{-}(H_2O)_6$ anionic cluster with DNA are mediated by a single/double $H_2O$ layer, but on one occasion a direct H-bonding with a DNA nucleobase atom was identified; 4) MD simulations underline the complex nature and interrelated motion of all system components: DNA, $e^{-}_{aq}$, counterions and hydration water; 5) The close $e^{-}_{aq}$ approach to DNA perturbs significantly the double helix and evokes disruption of Watson-Crick H-bonding, as well as induces counterion displacement; 6) The BU6·A17 base pair is less disturbed and in the studied time frame of 2 ns, the $e^{-}_{aq}$ did not approach the brominated DNA strand, and particularly did not approach BUdR. This result may have important implications for understanding the inefficient radiosensitized damage of double-stranded BUdR-DNA.

**Acknowledgements** This work was supported by the Cancer Research Society (Canada).

## References


1. von Sonntag C (2006) Free Radical Induced DNA damage and repair: A chemical perspective, Springer, Berlin
2. Bernas A, Feradini C, Jay-Gerin JP (1996) Can J Chem 74:1–23
3. Clark T, Illing G (1987) J Am Chem Soc 109:1013–1020
4. Schnitker J, Rossky PJ (1989) J Phys Chem 93:6965–6969
5. Pommeret S, Gauduel Y (1991) J Phys Chem 95:4126–4130
6. Tachikawa H, Lund A, Ogasawara M (1993) Can J Chem 71:118–124
7. Wong KF, Rossky PJ (2001) J Phys Chem A 105:2546–2556
8. Sommerfield T, Jordan KD (2006) J Am Chem Soc 128:5828–5833
9. Coe JV, Lee GH, Eaton JG, Arnold ST, Sarkas HW, Bowen KH, Ludewigt C, Haberland H, Worsnop DR (1990) J Chem Phys 92:3980–3982
10. Kim J, Becker I, Cheshnovsky O, Johnson MA (1998) Chem Phys Lett 297:90–96
11. Kelley JA, Weddle GH, Robertson WH, Johnson MA (2002) J Chem Phys 116:1201–1203
12. Tauber MAJ, Mathies RA (2003) J Am Chem Soc 125:1394–1402
13. Symons MCR (1988) J Phys Chem 92:7260–7262
14. Schlick S, Narayana PA, Kevan L (1976) J Chem Phys 64:3153–3160
15. Feng D-F, Kevan L (1980) Chem Rev 80:1–20
16. Boudaiffa B, Cloutier P, Hunting DJ, Huels MA, Sanche L (2000) Science 287:1658–1660
17. Wagenknecht H-A (2003) Angew Chem Int Ed 42:2454–2460
18. Manetto A, Breeger S, Chatgilialoglu C, Carell T (2006) Angew Chem Int Ed 45:318–321
19. Cai Z, Sevilla MD (2000) J Phys Chem B 104:6942–6949
20. Cook GP, Greenberg MM (1996) J Am Chem Soc 118:10025–10030
21. Fuciarelli AF, Sisk EC, Zimbrick JD (1994) Int J Radiat Biol 65:409–418
22. Nese C, Yuan Z, Schuchmann MN, von Sonntag C (1992) Int J Radiat Biol 62:527–541
23. Colson AO, Sevilla MD (1995) Int J Radiat Biol 67:627–645
24. Cecchini S, Girouard S, Huels MA, Sanche L, Hunting DJ (2004) Rad Res 162:604–615
25. Cecchini S, Girouard S, Huels MA, Sanche L, Hunting DJ (2005) Biochem 44:1932–1940
26. Dextraze M-E, Wagner RJ, Hunting DJ (2007) Biochem 46:9089–9097
27. Gantchev TG, Cecchini S, Hunting DJ (2005) J Mol Model 11:141–159
28. Young MA, Ravishanker G, Beveridge DL (1997) Biophys J 73:2313–2336
29. Westhof E, Rubin-Carrez C, Fritsch V (1995) In: Goodfellow JM (ed) Computer modelling in molecular biology, Chapter 5. Wiley VCH, Weinheim, pp 101–131
30. Berendsen HJC, Postma JPM, van Gunsteren WF, DiNola A, Haak JR (1984) J Chem Phys 81:3684–3690
31. Essman U, Perera L, Berkowitz ML, Darden T, Lee H, Pedersen L (1995) J Chem Phys 103:8577–8593
32. Beveridge DL, Ravishanker G (1994) Curr Opin Struct Biol 4:246–255
33. Kollman PA, Dixon R, Cornell W, Fox T, Chipot C, Pohorille, A (1997) 3:83–96 The development/application of a "minimalist" organic/biochemical molecular mechanic force field using a combination of ab initio calculations and experimental data In: Wilkinson A, Weiner N, van Gunsteren W (eds.) Computer simulations of biomolecular systems: Theoretical and experimental applications
34. Bonvin AMJJ, Sunnerhagen M, Otting G, van Gunsteren WF (1998) J Mol Biol 282:859–873
35. Feig M, Montgomery Pettitt B (1999) J Mol Biol 286:1075–1095
36. Várnai P, Zakrzewska K (2004) Nucl Acids Res 32:4269–4280
37. Sherer EC, Cramer CJ (2004) Theor Chem Acc 111:311–327
38. Schmidt KH, Han P, Bartels DN (1995) J Phys Chem 99:10530–10539
39. Feig M, Pettitt BM (1998) Biophys J 75:134–149
40. Koneshan S, Rasaiah JC, Lynden-Bell RNM, Lee SH (1998) J Phys Chem B 102:4193–4204
41. Marcus RA (1998) Acta Chem Scand 52:858–863
42. Bertran J, Gallardo I, Moreno M, Savéant J-M (1992) J Am Chem Soc 114:9576–9583
43. Close DM (2004) J Phys Chem A 108:10376–10379
44. Gaballah ST, Collier G, Netzel TL (2005) J Phys Chem B 109:12175–12181
45. Schröder C, Rudas T, Boresch S, Steinhauser O. J. Chem. Phys 124:234907–234907
46. Pearson RG (1989) J Org Chem 54:1423–1430
47. Gantchev TG, van Lier JE, Hunting DJ (2005) Rad Phys Chem 72:367–379
48. Yoon C, Prive GG, Goodsell DS, Dickerson RE (1988) Proc Natl Acad Sci USA 85:6332–6336
49. Umezawa Y, Nishio M (2002) Nucl Acid Res 30:2183–2192